A Numerical Study of the Behavior of Concrete Columns constructed with Recycled Aggregate reinforced with GFRP Rebars

Ahlam Sader Mohammed
Department of Civil Engineering, College of Engineering, University of Technology, Baghdad, Iraq
40159@uotechnology.edu.iq (corresponding author)

Bashar F. Abdulkareem
Department of Reconstruction and Projects, University of Baghdad, Baghdad, Iraq
b.faisal1101@coeng.uobaghdad.edu.iq

Received: 13 November 2024 | Revised: 3 December 2024 and 8 December 2024 | Accepted: 14 December 2024

 DOI: https://doi.org/10.48084/etasr.9600

ABSTRACT

This research presents the findings of a numerical simulation conducted using the ABAQUS/CAE Finite Element (FE) software, with the purpose of investigating the behavior of short concrete columns constructed using recycled aggregate reinforced by Glass Fiber Reinforced Polymer (GFRP) bars. The numerical validation technique included an analysis of the experimental data of twenty columns constructed utilizing recycled aggregate reinforced by steel or GFRP rebars. Additional aspects, such as the column length, acting as an indicator of column slenderness, and the configuration of the column section, were also investigated. The results revealed a significant correlation between the failure loads and axial displacement of the computational models and those derived from the experimental methods. It was found that the increase in the column length was inversely proportional to its load carrying capacity. The drop percentage in the load carrying capacity was 6% and 11% for columns with length of 1100 mm and 1500 mm, respectively, compared to the reference square column with 700 mm length. The drop percentage in the load carrying capacity was 6.9% and 12.7% for columns with lengths of 1100 mm and 1500 mm, respectively, compared to the reference circle column with 700 mm length.

Keywords-GFRP bars; concrete columns; circular section; recycled aggregate; section configuration; ABAQUS

I. INTRODUCTION

Concrete columns are essential components in the design and construction of many structures and buildings. However, they can be damaged by various factors, including high-impact forces, such as shocks, explosions, and earthquakes, as well as changes in the structural use, corrosion, and chemical reactions [1-5]. Numerous building projects in Iraq have either completed their planned lifespan or have not been constructed based on urban development standards. Several of them have been also destroyed because of warfare. The demolition and maintenance of these structures produce a significant quantity of concrete waste. The environmental legislation and increasing expenses associated with the natural aggregate production come along with new regulations and recommendations in several Western nations [6]. The limited corrosion resistance of the steel reinforcement and the need to enhance the durability of reinforced concrete structures have led to the adoption of GFRP bars in building construction [7]. Authors in [8] examined the compressive characteristics of reinforced concrete columns constructed from recycled material and subjected to monotonic uniaxial stress. Seventeen columns of diverse kinds, qualities, and quantities of recycled coarse and fine aggregates were evaluated. The columns were analyzed for their failure mechanisms, compressive strength, and ductility. The maximum compressive strength of the columns was specifically compared to the formulae provided by the American Concrete Institute (ACI) 318-08. A comparison of the test results with the computed strengths for the axial load capacity of the RAC columns, utilizing the aforementioned methodology, demonstrated that the RAC columns meet the ACI design strength standards. Authors in [9] presented the findings of experimental and computational studies regarding the structural behavior of GFRP pultruded columns exposed to minor eccentric loads about the major (strong) axis. Three series of 1.50 m long GFRP I-section columns (120 mm × 60 mm × 6 mm) were subjected to compressive testing with eccentricity-to-height (e/h) ratios of 0, 0.15, and 0.30. It was determined that minor eccentricity significantly influences the behavior of GFRP pultruded columns. The initial axial rigidity of eccentrically laden columns was comparable to that of concentrically loaded columns. However, as the loads

increased, the stiffness significantly diminished due to bending and second-order P–δ effects. The outcomes from the experimental program were juxtaposed with analytical forecasts and numerical simulations employing the Finite Element Method (FEM) and the Generalized Beam Theory (GBT). A strong concordance was achieved between the experimental data and both the analytical and numerical findings. Authors in [10] performed an experimental and theoretical study on short concrete columns reinforced with GFRP to clarify the compressive behavior of GFRP bars. The experimental program included fourteen specimens, each measuring 500 mm in length with a square cross-section of 150 mm × 150 mm, consisting of nine GFRP-reinforced specimens (6#5) and five plain concrete specimens. The specimens were subjected to testing under concentric and eccentric compressive stresses until failure ensued. Three eccentricity-to-width ratios, 0.1, 0.2, and 0.3, were investigated, with the eccentricities having been symmetrically applied at both ends of the simply supported columns. The testing program revealed that the GFRP bars did not undergo crushing at the peak load, and the corresponding strain did not reach the 50% of the crushing capacity established from the material test. An analytical model was developed and verified with the experimental test data. The model incorporated both material nonlinearity and geometric nonlinearity. A parametric study was performed utilizing the model to assess the impact of eccentricity, reinforcement ratio, and concrete strength, which confirmed the capability of the GFRP bars to withstand substantial pressures beyond their compressive strain limit.

Authors in [11] investigated the characteristics of concrete by substituting coarse aggregate with destroyed column trash in varying quantities of 10%, 20%, 30%, 40%, 50%, and 100%. The ages of the analyzed samples were 7, 14, and 28 days. The findings indicate that the compressive strength exceeded 30 N/mm^2 when up to 30% of fresh coarse aggregate was substituted. The compressive strength was recorded at 27.11 N/mm^2 with a 50% replacement, above the target value of 26.6 N/mm^2. Consequently, routine construction operations are more appropriate for this concrete, which may be substituted by up to 50%. Authors in [12] demonstrated the use of FE analysis to predict the behavior of GFRP-reinforced geopolymer and conventional Portland cement concrete columns under concentric and eccentric axial stresses, employing experimental data for validation. The commercial numerical analysis software ABAQUS was employed. The experimental curves closely matched the expected load-displacement responses. The expected N-M strength interaction graphs aligned with the experimental data, particularly for the GFRP RC columns with considerable spacing between the ligatures, as they exhibited ductile failure accurately depicted by the computational model. Authors in [13] examined the performance of columns subjected to axial loads composed of recycled aggregates. The primary variables under examination were the effects of the steel fibers, with volumes varying from 0% to 2%, on the composition of concrete and the proportion of recycled aggregates in the concrete mix. The experimental results indicated that the proportion of the recycled particles in concrete influences its strength. The load bearing capacity of the concrete columns containing over 30% recycled aggregate was enhanced using steel fibers.

Authors in [14] examined the longitudinal compressive behavior of GFRP columns by constructing and evaluating five columns subjected to axially concentric load. The concrete comprised a pair of fibers. Two types of transversal restriction (GFRP rings and GFRP swirls) were employed. The results indicate that GFRP columns encased in GFRP swirls have enhanced longitudinal rigidity and ductility characteristics.

Authors in [15] examined the impact of recycled materials on the performance of linked with fibre rectangular RC columns. The research shown that the integration of 50% natural aggregates with 50% recycled aggregates led to decreases of 10%, 18%, 30%, and 22% in compressive strength, splitting tensile strength, flexural strength, and modulus of elasticity, respectively. Substituting 100% of conventional aggregates with 100% of recycled aggregates led to reductions of 30%, 35%, 58%, and 63%, respectively.

II. RESEARCH SIGNIFICANCE

The current study aims to develop a simulation model capable of predicting the behavior of short concrete columns made with recycled aggregate and being reinforced with GFRP bars.

III. TEST SPECIMENS

The experimental program presented in [6] involved testing 20 short columns under monotonic concentric compression loads. The procedure included casting 20 columns with cross-sectional dimensions of 150 mm × 150 mm and a length of 700 mm. Of these, 10 columns were reinforced with 8 mm diameter steel bars, while the remaining specimens were reinforced with 10 mm diameter GFRP rebars. All specimens were reinforced with steel ties of a 6 mm diameter. Table I delineates the specifics of the evaluated columns. Figure 1 illustrates the characteristics of the evaluated short columns, Table II outlines the results of the ten concrete mix properties, Table III depicts the steel bars' properties, and Table IV shows the GFRP bars' properties.

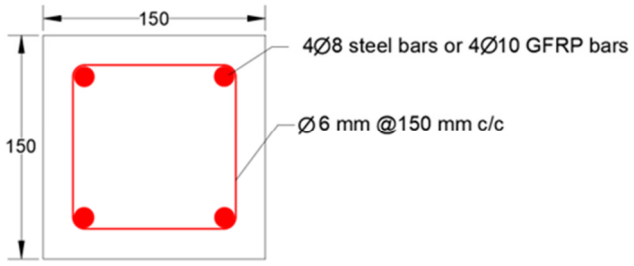

Fig. 1. Details of the samples.

IV. MODELING AND ANALYSIS OF THE TESTED COLUMNS IN ABAQUS

The present research uses the FEM to analyze columns via the implementation of the ABAQUS CAE version 2019 computer program, specifically applying the Standard/Explicit Model. The structural study of all columns was conducted

deploying a single-step approach, and specifically static analysis. The concrete columns and steel capital were simulated utilizing the isoperimetric eight-node brick element (C3D8R). The three-dimensional two-node bar component with 3-dimensional movements in the x, y, and z axes, known as the truss element (T3D2), was used for the reinforced steel bars or CFRP bars. To thoroughly analyze all specimens within the ABAQUS simulation framework, multiple components were created, as illustrated in Figure 2.

TABLE I. DETAILS OF TESTING COLUMNS

Column designation	Concrete aggregate type	Percentage of replaced aggregate (%)	Main bars type
N-Sto-0	Normal	-	Steel
A50-Sto-0	DRA	50	Steel
A50-Sto-1	DRA	50	Steel
A50-St1o-1	DRA	50	Steel
C50-St1o-1	DRC	50	Steel
A100-Sto-0	DRA	100	Steel
C100-Sto-0	DRC	100	Steel
A100-Sto-1	DRA	100	Steel
A100-St1o-1	DRA	100	Steel
C100-St1o-1	DRC	100	Steel
N-Gfo-0	Normal	-	GFRP
A50-Gfo-0	DRA	50	GFRP
A50-Gfo-1	DRA	50	GFRP
A50- Gf1o-1	DRA	50	GFRP
C50-Gf1o-1	DRC	50	GFRP
A100-Gfo-0	DRA	100	GFRP
C100-Gfo-0	DRC	100	GFRP
A100-Gfo-1	DRA	100	GFRP
A100-Gf1o-1	DRA	100	GFRP
C100-Gf1o-1	DRC	100	GFRP

TABLE II. RESULTS OF CONCRETE MIXES

Mix No.	Compressive strength fcu (MPa) after 28 days	Splitting tensile strength fct (MPa) after 28 days
1	41.8	3.553
2	37.6	3.379
3	39.1	3.488
4	40.6	3.499
5	38	3.39
6	35	3.245
7	33.7	3.194
8	35.1	3.259
9	36.7	3.325
10	36.1	3.303

TABLE III. TENSILE TEST OF REINFORCEMENT STEEL BARS

Rebar diameter (mm)	Area of the sectional shape (mm²)	Fy (MPa)	Fu (MPa)	Total elongation (%)
6	27.3	420	465	9.29
8	50.3	583	672	12.33

TABLE IV. TEST OF GFRP REBAR

Ø (mm)	Section area (mm²)	Modulus of elasticity (MPa)	Minimal tensile strength (MPa)	Elongation (%)	Tensile strength upon rupture (MPa)
10.0	79	79325	751	2.49	1206.9

The support on the bottom of the column is modeled as fixed by restricting the nodes. Figure 3 displays the boundary constraints and load specifications.

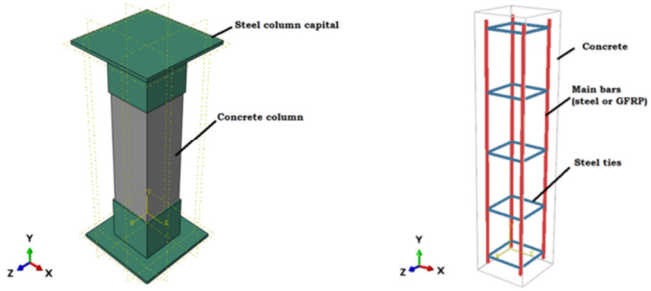

Fig. 2. Creating parts and assembly in ABAQUS.

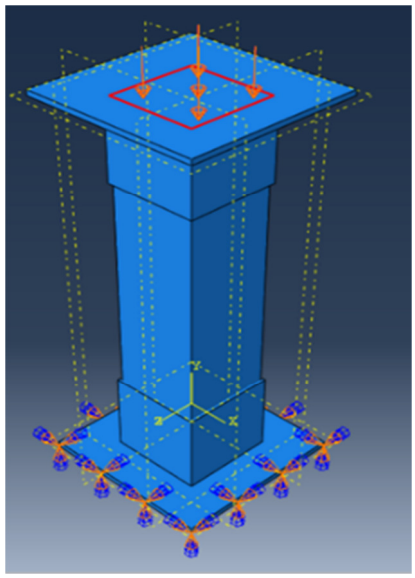

Fig. 3. Conditions of boundaries and loads utilized in the analysis.

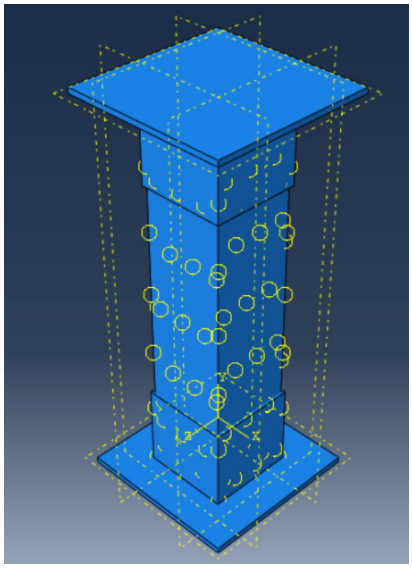

Fig. 4. Interaction between parts.

For a comprehensive assessment of the part interaction, the primary bars and steel links are regarded as fully encased in concrete. An interaction constraint of type Tie was applied between the concrete column and steel capital, as it can be seen in Figure 4. Table V illustrates the input data for the concrete damage plasticity, while Tables VI and VII portray the compressive and tension data, respectively, for mix1, according to [6].

TABLE V. INPUT INFORMATION FOR CONCRETE DAMAGE PLASTICITY

Elasticity modulus	Poisson' ratio	Dilation angle	Eccentricity	$\epsilon_{bo}/\epsilon_{co}$	Viscosity
27348	0.18	35	1.16	0.667	0

TABLE VI. MIX1 COMPRESSIVE DATA

Yield stress (MPa)	Inelastic strain
13.4553041	0
19.59707686	2.69267E-05
24.93355506	8.45998E-05
29.04493045	0.000185565
31.82370468	0.000332247
33.39063955	0.000527755
33.858	0.000761965
32.51403824	0.001306108
29.50451562	0.001920153
26.05622962	0.002547241
22.78410928	0.003161888
19.81818065	0.003774338
17.28402825	0.004368001
9.459073674	0.007129124
5.804497163	0.009782756
3.913337377	0.012356907
2.822557822	0.014871792
2.12055603	0.017417461
1.653308258	0.019939546

TABLE VII. MIX1 TENSION DATA

Yield stress (MPa)	Strains
3.553	0
2.242366195	0.000147478
1.677911797	0.000267972
0.998968363	0.000592623
0.731207608	0.000902345
0.51809997	0.001410082
0.407536831	0.001914097
0.3389118	0.002416588
0.291776699	0.0029183
0.257211437	0.003419555
0.230673268	0.003920518
0.119612169	0.008924551
0.083806979	0.013925851
0.065571225	0.018926513
0.054359492	0.02392692
0.046703349	0.028927198
0.04111097	0.033927401
0.036829501	0.038927556

V. CALIBRATION OF THE MANUFACTURED FINITE ELEMENT MODEL

This section presents several comparisons of the experimental results and pertinent numerical data. The factors of interest encompass the connection between the load and axial deflection during the application of external forces, the cracking at failure, and the evaluation of the load and axial deflection at the failure stage.

A. Load vs Axial Deflection Relation

Figures 5 and 6 demonstrate comparisons of the load versus the axial deflection relation between the experimental and numerical results for all GFRP and steel columns, respectively. The computer models had higher axial stiffness than the data derived from the experiments regarding both the linear and nonlinear behavior, but an acceptable degree of concordance was observed between the two of them. The computer models demonstrated greater stiffness than the actual data across all behavioral zones, albeit there was satisfactory concordance between the two of them.

(a)

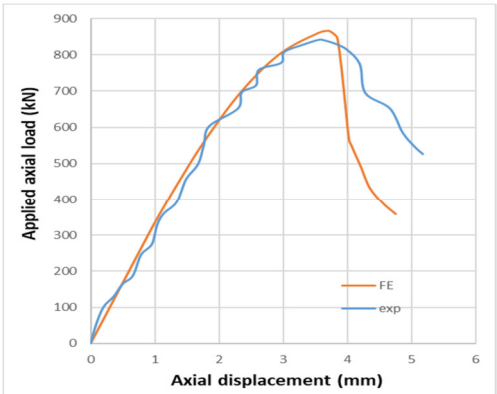

(b)

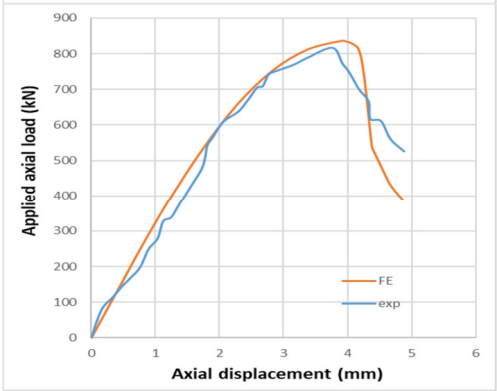

(c)

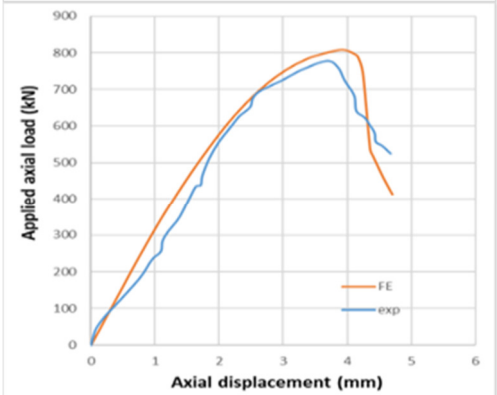

(d)

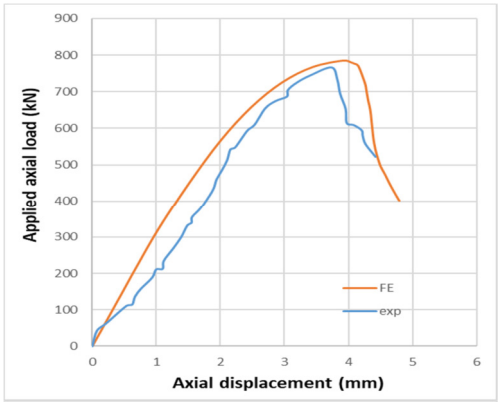

(e)

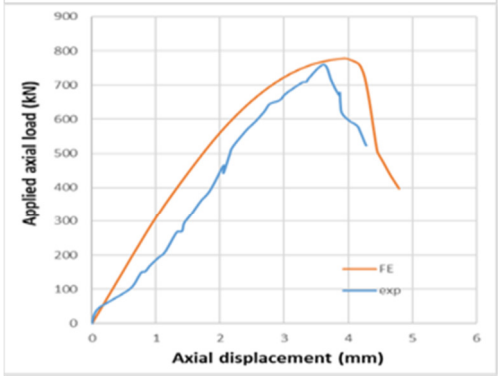

(f)

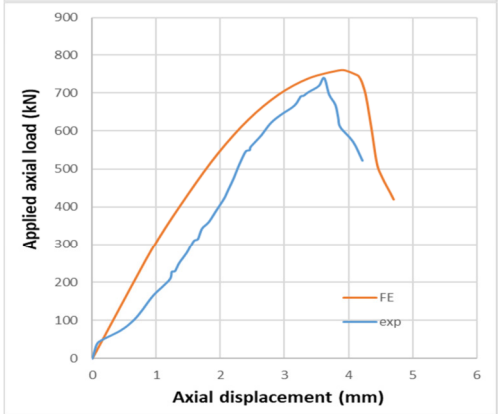

(g)

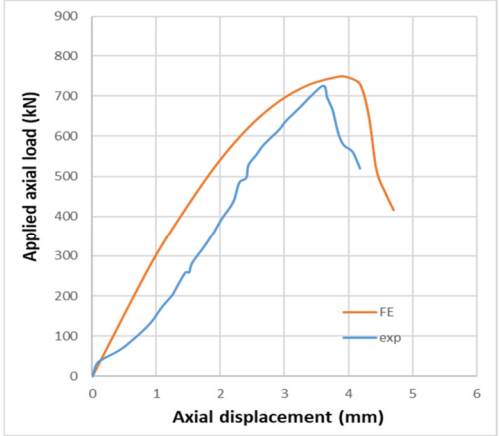

(h)

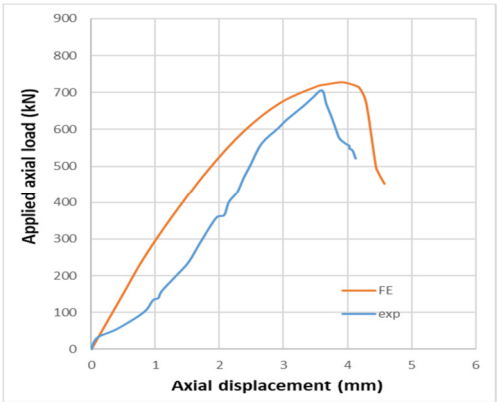

(i)

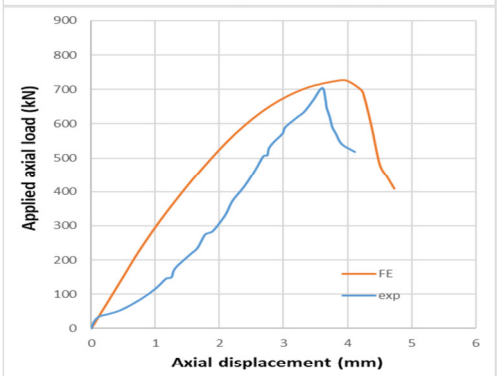

(j)

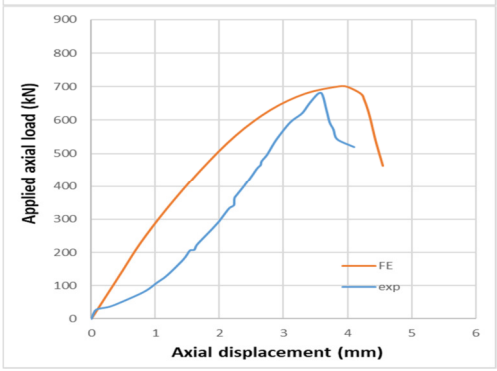

Fig. 5. Experimental and numerical load versus axial deflection for GFRP columns. (a) N-Gfo-0, (b) A50- Gf1o-1, (c) A50-Gfo-1, (d) C50-Gf1o-1, (e) A50-Gfo-0, (f) A100-Gf1o-1, (g) C100-Gf1o-1, (h) A100-Gfo-1, (i) A100-Gfo-0, (j) C100-Gfo-0.

(a)

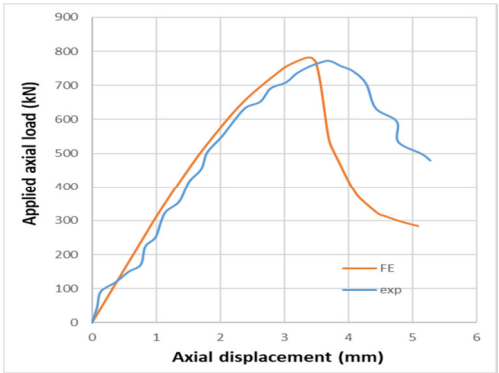

(b)

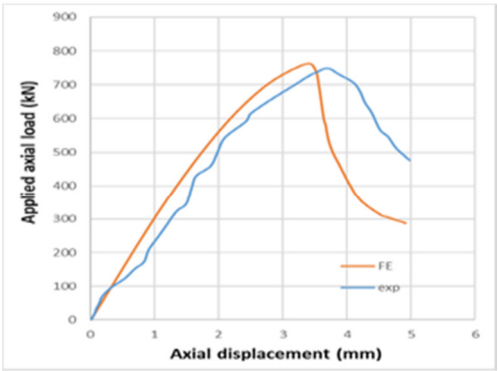
Applied axial load (kN)
Axial displacement (mm)
FE
exp

(c)

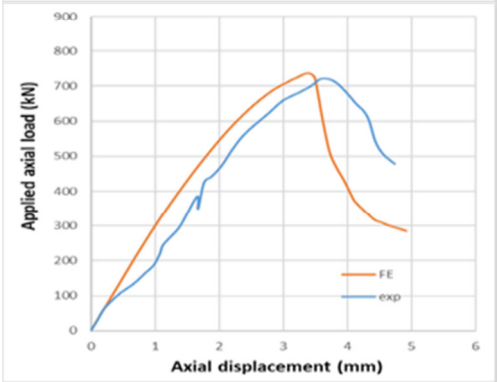
Applied axial load (kN)
Axial displacement (mm)
FE
exp

(d)

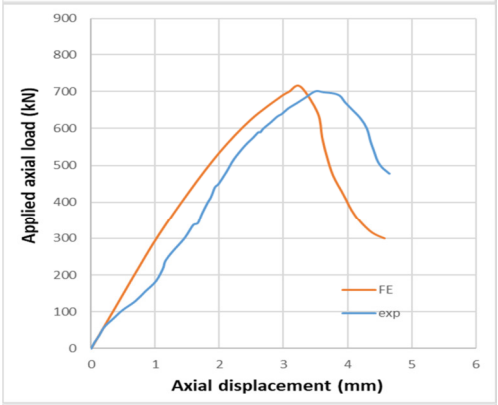
Applied axial load (kN)
Axial displacement (mm)
FE
exp

(e)

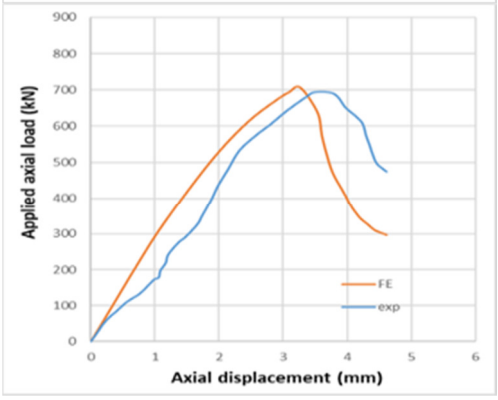
Applied axial load (kN)
Axial displacement (mm)
FE
exp

(f)

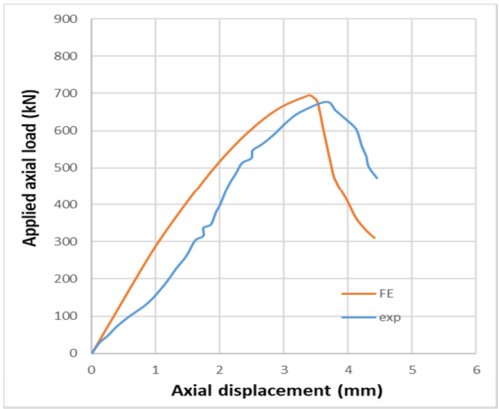
Applied axial load (kN)
Axial displacement (mm)
FE
exp

(g)

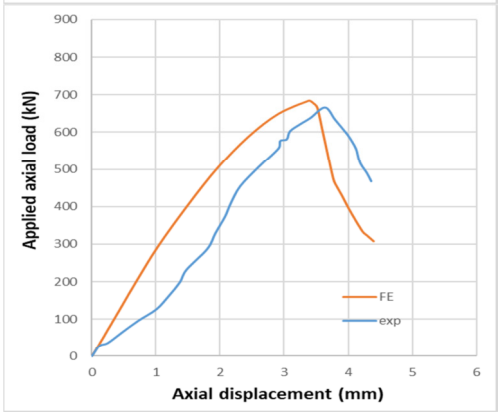
Applied axial load (kN)
Axial displacement (mm)
FE
exp

(h)

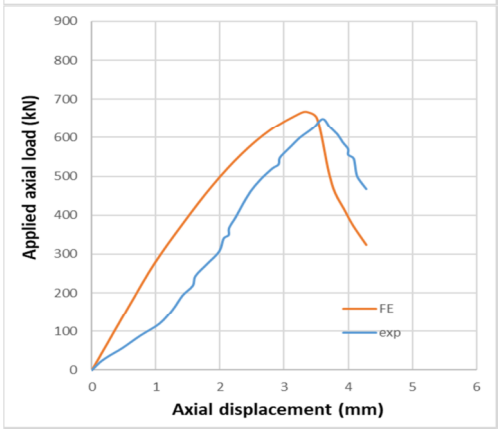
Applied axial load (kN)
Axial displacement (mm)
FE
exp

(i)

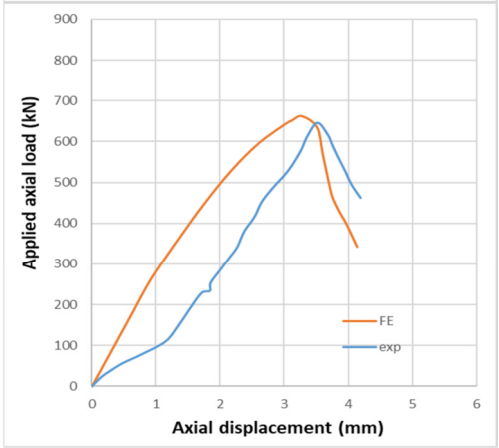
Applied axial load (kN)
Axial displacement (mm)
FE
exp

(j)

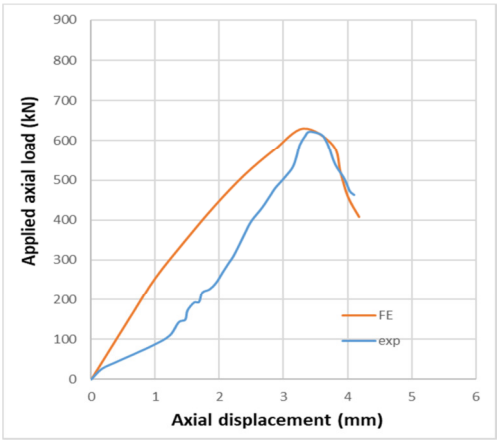

Fig. 6. Experimental and numerical load versus axial deflection for steel columns. (a) N-Sto-0, (b) A50- St1o-1, (c) A50-Sto-1, (d) C50-st1o-1, (e) A50-Sto-0, (f) A100-St1o-1, (g) C100-St1o-1, (h) A100-Sto-1, (i) A100-Sto-0, (j) C100-Sto-0.

B. Load and Axial Deflection at Failure Stage

Table VIII shows a detailed comparison between the results of the experiments taken at the failure phase and the load that failed and axially deflection calculated using the FE model for each column that underwent axially compression examination. Results from testing with experiments and computer models showed a high degree of agreement with regard to the final load and axially deflection. For example, the mean of the coefficient of variation for (Pu)FE/(Pu)Exp for the final loads was 0.62% and the value of the mean was 1.025, while, for the axial deflection (Δu FE / Δu Exp) they were 0.988 and 6.92%, respectively.

The FE evaluation findings demonstrate that the models possess more axial stiffness than the experimental specimens, as seen by the load-axial deflection relation. Multiple variables could have contributed to the heightened stiffness in the FEM study results. During the experiment, the concrete exhibited small fissures, which may have resulted from the drying shrinkage and curing processes. These conditions could lead to a decrease in the specimen's stiffness.

The first assumption in the analysis of finite elements is the belief that the joint between GFRP and concrete is flawless. It is possible that the actual specimen defies this notion. A breakdown in the combination of activity between GFRP and concrete occurs when connections slip. Consequently, the overall stiffness of the real sample can be inferior to expectations derived from FE analysis [16].

C. Cracking at Failure

Figure 7 displays a contour graphic depicting the maximum plastic strain in the analyzed columns, along with the crack patterns of the experimental columns at the ultimate stage. This visualization highlights the impact of loads on the strain concentrations and crack development. A strong correlation between the numerical and experimental crack patterns can be observed.

TABLE VIII. EXPERIMENTAL AND NUMERICAL FAILURE LOAD AND MID-SPAN DEFLECTION

Column ID	Ultimate load (Pu)			Axial deflection at ultimate load (Δu)		
	EXP(kN)	F.E. (kN)	FE/EXP	EXP (mm)	F.E. (mm)	FE/EXP
N-Sto-0	771.4	782.6	1.014519	3.7	3.41	0.921
A50-Sto-0	694.26	706	1.01691	3.5	3.266	0.933
A50-Sto-1	721.26	736.9	1.02168	3.6	3.37	0.936
A50-St1o-1	749.03	762.6	1.018116	3.7	3.373	0.911
C50-St1o-1	701.2	712.9	1.016685	3.5	3.266	0.933
A100-Sto-0	645.9	662.3	1.02539	3.51	3.277	0.933
C100-Sto-0	621.75	630	1.01326	3.4	3.316	0.975
A100-Sto-1	647.98	666.8	1.029044	3.6	3.343	0.928
A100-St1o-1	677.29	695.3	1.026591	3.66	3.381	0.923
C100-St1o-1	666.5	684.97	1.02771	3.64	3.381	0.928
N-Gf0-o	842.45	866.2	1.028191	3.56	3.703	1.04
A50-Gfo-0	760	777.7	1.023289	3.62	3.926	1.084
A50-Gfo-1	777.5	807	1.037942	3.68	3.876	1.053
A50- Gf1o-1	817	836.9	1.024357	3.76	3.919	1.042
C50-Gf1o-1	766.5	785.6	1.02491	3.73	3.926	1.051
A100-Gfo-0	705.4	726.3	1.029628	3.6	3.876	1.076
C100-Gfo-0	680	700.8	1.03058	3.59	3.876	1.079
A100-Gfo-1	706	728.3	1.03158	3.6	3.878	1.077
A100-Gf1o-1	740	759.2	1.025945	3.62	3.852	1.064
C100-Gf1o-1	726	747.4	1.029476	3.61	3.852	1.067
Average			1.025	Average		0.998
Standard deviation			0.006341	Standard deviation		0.0690708
Coefficient of variation (%)			0.62	Coefficient of variation (%)		6.92

VI. NUMERICAL PARAMETRIC STUDY

Considering the preceding verification of the FE evaluation for the experimental data obtained in this work, a comprehensive parametric study was performed using the FE model. The investigation parameters are the ratio of column length/section width (L/h) and the section configuration (square with width=150 mm or circle with diameter=169 mm) to get the same section area. An old model (N-Gfo-0) with GFRP bars and normal concrete was used as a reference sample for this parametric study in addition to five new models, as shown in Table IX. Figure 8 displays the simulation of the circle column, while Figure 9 illustrates the parametric study samples.

The effect of changing the length of the column on the load versus axial deflection relationship is depicted in Figure 10. Each figure has 3 columns with the same section properties but different lengths. From the load versus the deflection curves, it is evident that the columns exhibit equal stiffness throughout the elastic range after the occurrence of cracking. Then the columns with a higher length have smaller axial stiffness. The effect of changing the shape of the column section on the load versus the axial deflection relationship is displayed in Figure 11.

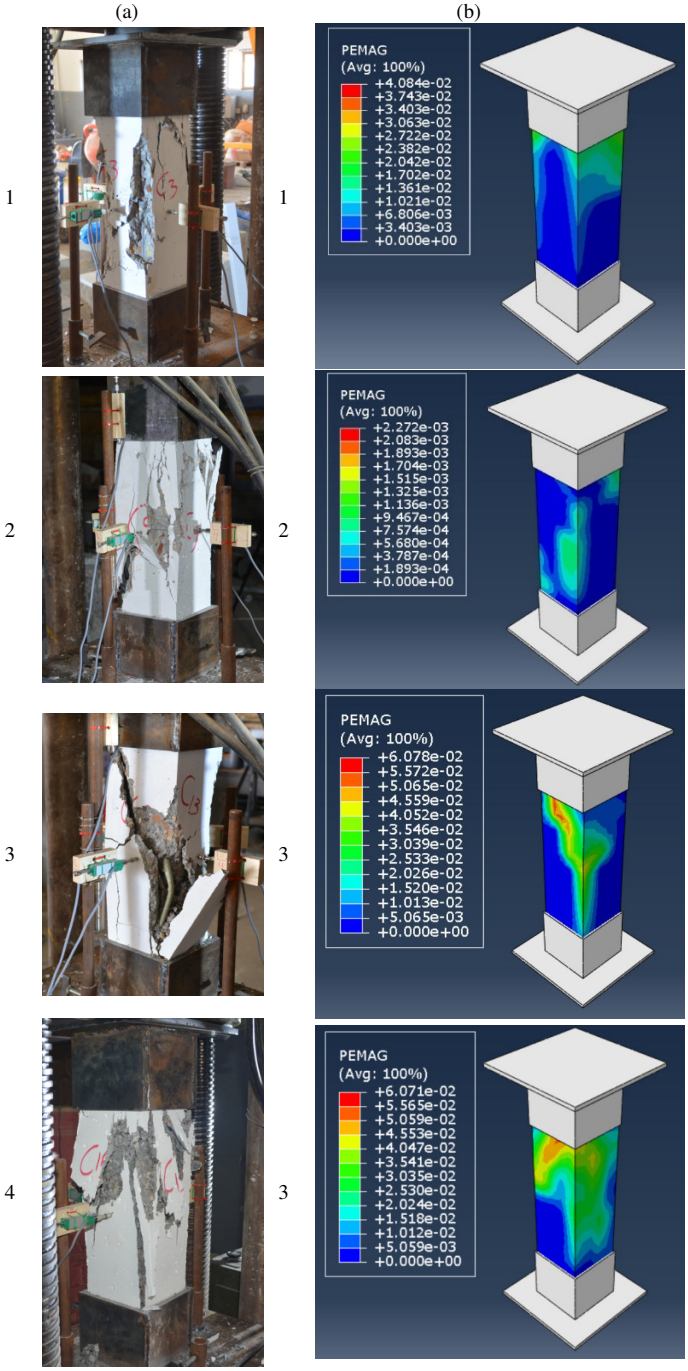

Fig. 7. Ultimate damage result of the numerical ABAQUS and experimental model for some samples. (a) 1.A50-Sto-1-Experimental, 2.A100-St1o-1-Experimental, 3.A50-Gfo-1-Experimental, 4.C50-Gf1o-1-Experimental. (b) 1.A50-Sto-1-Numerical, 2.A100-St1o-1-Numerical, 3.A50-Gfo-1-Numerical, 4.C50-Gf1o-1-Numerical.

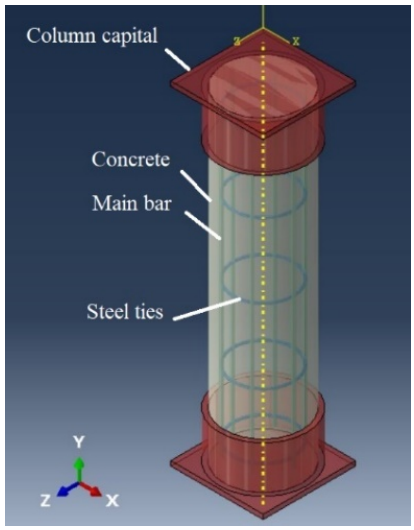

Fig. 8. Creating parts and assembly of circle column.

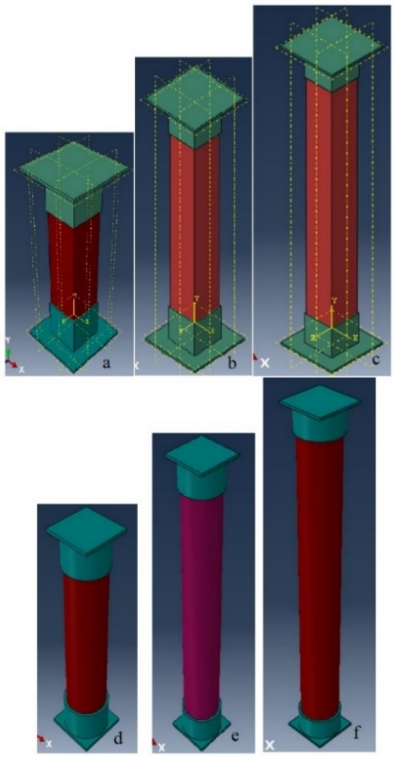

Fig. 9. Parametric study samples (a-square and L=700 mm, b-square and L=1100 mm, c-square and L=1500 mm, d-circle and L=700 mm, e-circle and L=1100 mm, f-circle and L=1500 mm).

TABLE IX. BEAM DETAILS FOR NUMERICAL PARAMETRIC STUDY

Column designation	Section configuration	Length of column (mm)	L/h
N-Gfo-0	square	700	4.67
S1100	square	1100	7.33
S1500	square	1500	10
C700	circle	700	4.14
C1100	circle	1100	6.51
C1500	circle	1500	8.88

(a)

(b)

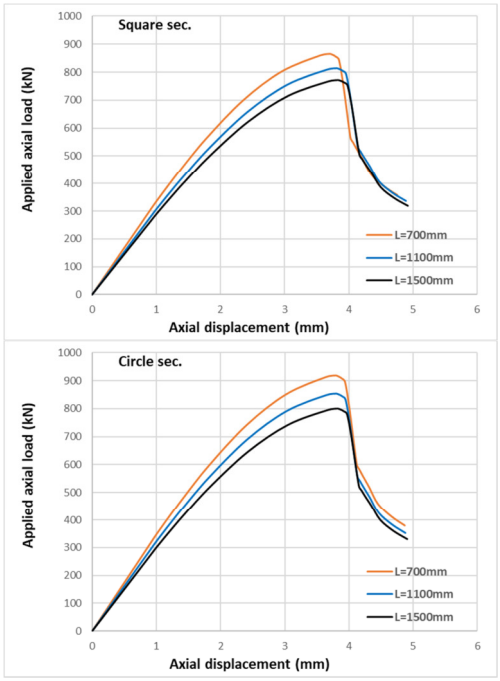

Fig. 10. (a) Square sections,(b) Circle sections. Impact of changing the length of the column on load versus axial deflection relationship.

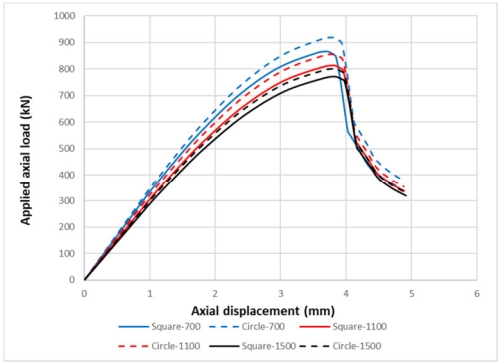

Fig. 11. Impact of changing the shape of column section on load versus axial deflection relationship.

TABLE X. EFFECT OF CHANGING THE LENGTH OF COLUMN ON LOAD CARRYING CAPACITY

Column ID	Section shape	Column length (mm)	Load carrying capacity Pu (kN)	Decrease percent of Pu (%)
N-Gfo-0	Square	700	866.2	Reference
S1100	Square	1100	814	6
S1500	Square	1500	771	11
C700	Circle	700	918.1	Reference
C1100	Circle	1100	855	6.9
C1500	Circle	1500	801.8	12.7

The circular shape slightly enhances the stiffness of the column, even when the cross-sectional area and reinforcement area remain equal. Table X demonstrates the effect of changing the column length on the load carrying capacity, while Table XI highlights the effect of altering the column section shape on the load carrying capacity. Switching the section shape from square to circular resulted in an increase in the load carrying capacity by 6%, 5.03%, and 4% for the columns with lengths of 700 mm, 1100 mm, and 1500 mm, respectively. These findings align with the conclusions drawn in [17, 18].

TABLE XI. EFFECT OF CHANGING THE SHAPE OF COLUMN SECTION ON LOAD CARRYING CAPACITY

Column ID	Section shape	Column length (mm)	Load carrying capacity Pu (kN)	Increase percent of Pu (%)
N-Gfo-0	Square	700	866.2	Reference
C700	Circle	700	918.1	6
S1100	Square	1100	814	Reference
C1100	Circle	1100	855	5.03
S1500	Square	1500	771	Reference
C1500	Circle	1500	801.8	4

VII. CONCLUSIONS

- A strong correlation was identified between the final loads and the axial movement of computerized models compared to those derived from experimental approaches. The average and percentage of variation for the percentage of final loads (Pu)FE/(Pu)Exp were determined as 1.011 and 1.336%, respectively. The average and percentage of variation for the ratio of axially movement (δ FE / δ Exp) were found to be 0.928 and 3.464%, respectively
- Increasing the length of the column is inversely proportional to the load carrying capacity. The drop percentage in the load carrying capacity was 6% and 11% for columns with a length of 1100 mm and 1500 mm, respectively, compared to the reference square column with a 700 mm length. The drop percentage in the load carrying capacity was 6.9% and 12.7% for columns with a length of 1100 mm and 1500 mm, respectively, compared to the reference circle column with a 700 mm length.
- The circular shape slightly enhances the stiffness of the column, even though the cross-sectional area and reinforcement area are the same. Changing the section shape from square to circular resulted in an increase in the load carrying capacity by 6%, 5.03%, and 4% for the columns with lengths of 700 mm, 1100 mm, and 1500 mm, respectively.

REFERENCES

[1] C. Zeng, P. Cui, Z. Su, Y. Lei, and R. Chen, "Failure modes of reinforced concrete columns of buildings under debris flow impact," *Landslides*, vol. 12, no. 3, pp. 561–571, Jun. 2015, https://doi.org/10.1007/s10346-014-0490-0.

[2] M. Oad, A. H. Buller, B. A. Memon, N. A. Memon, and S. Sohu, "Flexural Stress-Strain Behavior of RC Beams made with Partial Replacement of Coarse Aggregates with Coarse Aggregates from Old Concrete: Part-2: Rich Mix," *Engineering, Technology & Applied Science Research*, vol. 8, no. 5, pp. 3338–3343, Oct. 2018, https://doi.org/10.48084/etasr.2129.

[3] B. F. Abdulkareem, A. F. Izzet, and N. Oukaili, "Post-Fire Behavior of Non-Prismatic Beams with Multiple Rectangular Openings Monotonically Loaded," *Engineering, Technology & Applied Science Research*, vol. 11, no. 6, pp. 7763–7769, Dec. 2021, https://doi.org/10.48084/etasr.4488.

[4] A. S. Mohammed, A. S. J. Al-Zuheriy, and B. F. Abdulkareem, "An Experimental Study to Predict a New Formula for Calculating the Deflection in Wide Concrete Beams Reinforced with Shear Steel Plates,"

International Journal of Engineering, vol. 36, no. 2, pp. 360–371, Feb. 2023, https://doi.org/10.5829/ije.2023.36.02b.15.

[5] A. S. Mohammed, H. H. M. Al-Ghabawi, A. A. Mansor, and L. A. G. Yassin, "Numerical investigation of the effect of longitudinal steel reinforcement ratio on the ductility of concrete beams," *Open Engineering*, vol. 14, no. 1, Jan. 2024, https://doi.org/10.1515/eng-2022-0593.

[6] O. T. Mohammed and H. J. Mohammed, "Compressive Strength of Square Short Concrete Columns reinforced with GFRP Bars produced with Recycled Demolition Aggregate," *Engineering, Technology & Applied Science Research*, vol. 14, no. 5, pp. 17428–17437, Oct. 2024, https://doi.org/10.48084/etasr.8626.

[7] S. P. Tastani and S. J. Pantazopoulou, "Bond of GFRP Bars in Concrete: Experimental Study and Analytical Interpretation," *Journal of Composites for Construction*, vol. 10, no. 5, pp. 381–391, Oct. 2006, https://doi.org/10.1061/(ASCE)1090-0268(2006)10:5(381).

[8] W.-C. Choi and H.-D. Yun, "Compressive behavior of reinforced concrete columns with recycled aggregate under uniaxial loading," *Engineering Structures*, vol. 41, pp. 285–293, Aug. 2012, https://doi.org/10.1016/j.engstruct.2012.03.037.

[9] F. Nunes, M. Correia, J. R. Correia, N. Silvestre, and A. Moreira, "Experimental and numerical study on the structural behavior of eccentrically loaded GFRP columns," *Thin-Walled Structures*, vol. 72, pp. 175–187, Nov. 2013, https://doi.org/10.1016/j.tws.2013.07.002.

[10] K. Khorramian and P. Sadeghian, "Experimental and analytical behavior of short concrete columns reinforced with GFRP bars under eccentric loading," *Engineering Structures*, vol. 151, pp. 761–773, Nov. 2017, https://doi.org/10.1016/j.engstruct.2017.08.064.

[11] D. R. Hegde, A. H. Jakathi, and P. V. Vijaykumar, "A Study on Strength Characteristics of Concrete by Replacing Coarse Aggregate by Demolished Column Waste," *International Journal of Engineering Research*, vol. 7, no. 06, pp. 386–395, Jun. 2018.

[12] M. Elchalakani, A. Karrech, M. Dong, M. S. Mohamed Ali, and B. Yang, "Experiments and Finite Element Analysis of GFRP Reinforced Geopolymer Concrete Rectangular Columns Subjected to Concentric and Eccentric Axial Loading," *Structures*, vol. 14, pp. 273–289, Jun. 2018, https://doi.org/10.1016/j.istruc.2018.04.001.

[13] O. S. Farhan, "Effect of Use Recycled Coarse Aggregate on the Behavior of Axially Loaded Reinforced Concrete Columns," *Journal of Engineering*, vol. 25, no. 10, pp. 88–107, Sep. 2019, https://doi.org/10.31026/j.eng.2019.10.07.

[14] U. Rafique, A. Ali, and A. Raza, "Structural behavior of GFRP reinforced recycled aggregate concrete columns with polyvinyl alcohol and polypropylene fibers," *Advances in Structural Engineering*, vol. 24, no. 13, pp. 3043–3056, Oct. 2021, https://doi.org/10.1177/13694332211017997.

[15] J. K. Sahan and E. K. Sayhood, "Effect of recycled aggregate on behaviour of tied reinforced fibrous rectangular short columns," *IOP Conference Series: Earth and Environmental Science*, vol. 779, no. 1, Mar. 2021, Art. no. 012006, https://doi.org/10.1088/1755-1315/779/1/012006.

[16] D. I. Kachlakev, T. H. Miller, T. Potisuk, S. C. Yim, and K. Chansawat, "Finite element modeling of reinforced concrete structures strengthened with FRP laminates : final report," Oregon. Dept. of Transportation. Research Group, FHWA-OR-RD-01-XX, May 2001.

[17] S. Guler, A. Çopur, and M. Aydogan, "A Comparative Study on Square and Circular High Strength Concrete-Filled Steel Tube Columns," *Advanced Steel Construction*, vol. 10, no. 2, pp. 234–247, Feb. 2013, https://doi.org/10.18057/IJASC.2014.10.2.

[18] R. El-Hacha and M. A. Mashrik, "Effect of SFRP confinement on circular and square concrete columns," *Engineering Structures*, vol. 36, pp. 379–393, Mar. 2012, https://doi.org/10.1016/j.engstruct.2011.12.006.